Estimation of Mobile Velocities and Direction of Movement in Mobile-to-Mobile Wireless Fading Channels

Alenka G. Zajić, *Member, IEEE*

***Abstract*— This paper proposes two new estimators, one for mobile velocities and one for direction of movement in mobile-to-mobile (M-to-M) wireless fading channels. First, we propose a new crossing-based estimator that jointly estimates velocities of both the transmitter and the receiver in M-to-M communications. Then, using the velocities estimator, we derive a new correlation-based estimator for the relative direction of movement of the transmitter and the receiver. The proposed estimators are designed for narrow-band wireless M-to-M communications. They are evaluated through extensive computer simulations, and the results show that the proposed algorithms provide very good estimation accuracy and perform well in the presence of non-isotropic scattering, line-of-sight propagation, and Gaussian noise.**

***Index Terms*— Velocity estimation, direction of movement estimation, mobile-to-mobile communications, fading channels.**

I. Introduction

The estimation of a mobile user's speed plays an important role in a variety of wireless applications. For example, it is used for energy-efficient routing in wireless networks [1], for mobility and resource management in wireless multimedia networks [2], for handoff, adaptive transmission, dynamic channel assignment, localization [3]-[6], etc. In the last two decades, a mobile user's speed estimation has been extensively studied in the literature, e.g., [6]-[13] and the reference therein. Speed estimation techniques can be classified into four major classes: crossing-based [6], [7], covariance-based [3], [10], [11], power spectrum-based [12], and maximum likelihood-based [5], [13] methods. Among these, crossing-based and covariance-based methods have low complexity and have been extensively used to estimate speed of the mobile user (relative to the fixed base-station).

In contrast to conventional wireless applications, where communication is between the fixed base-station and a mobile terminal, several emerging wireless applications require direct transmission between mobile terminals. Examples of these applications are mobile ad-hoc wireless networks, intelligent transportation systems, and relay-based cellular networks. In such mobile-to-mobile (M-to-M) communication systems, both the transmitter ($\mathrm{T_x}$) and receiver ($\mathrm{R_x}$) are in motion. While existing methods [6]-[13] can estimate relative velocity between two mobile terminals, some applications such as safety application or ad-hoc and energy-efficient routing, may require knowledge of both velocities, i.e., speeds of both the $\mathrm{T_x}$ and $\mathrm{R_x}$. Furthermore, these applications also require knowledge of the relative direction of movement of the $\mathrm{T_x}$ and $\mathrm{R_x}$. To the best of our knowledge, these problems have not been addressed in the open literature.

To address these issues, we first propose a new crossing-based estimator that jointly estimates velocities of both the $\mathrm{T_x}$ and $\mathrm{R_x}$. Then, using this *velocities estimator*, we propose a new correlation-based estimator that estimates the relative direction of the $\mathrm{T_x}$ and $\mathrm{R_x}$. These estimators are designed for narrow-band wireless M-to-M communications. The velocities are estimated by combining the number of zero-crossings and the number of maxima in the in-phase and quadrature components of the channel impulse response. We choose this crossing-based estimation approach because it does not depend on the type of propagation environment, i.e., it can be used in both urban surface streets and highway environments. Then, using the estimated velocities, the relative direction of movement of the $\mathrm{T_x}$ and $\mathrm{R_x}$ is estimated using the cross-correlation function between the in-phase and quadrature component of the channel impulse response. This approach leads to a simple closed-form expression for the estimation of the angle between the movement direction of $\mathrm{T_x}$ and the movement direction of $\mathrm{R_x}$ (i.e., the relative direction of movement of the $\mathrm{T_x}$ and $\mathrm{R_x}$).

The proposed algorithms are evaluated through extensive computer simulations with various system and channel parameters. In all simulations, we employ our single-input single-output (SISO) M-to-M channel simulator [14] because it matches measured data in a variety of urban environments, i.e., urban and highway environments [15]. These simulations show that the proposed algorithms provide very good estimation accuracy and perform well in the presence of a non-isotropic scattering, LoS propagation, and Gaussian noise. Finally, the results also show that, if used to estimate only one velocity, the proposed velocities estimator outperforms many of the crossing-, integral-, and covariance-based single-velocity estimators compared in [7].

The remainder of the paper is organized as follows. Section II describes M-to-M channel model. Section III derives the new crossing-based estimator that jointly estimates velocities of both the $\mathrm{T_x}$ and $\mathrm{R_x}$. Section IV derives the new correlation-based estimator for the relative direction of movement of the

Paper approved by Prof. Kainam Thomas Wong, the Associate Editor for IEEE Transactions on Vehicular Technology. Manuscript received July 7, 2011; revised October 24, 2011.

Alenka G. Zajić is with the School of Computer Science, Georgia Inst. of Tech., Atlanta, GA 30332 USA

$\mathrm{T_x}$ and $\mathrm{R_x}$. Section V presents the performance analysis of the proposed estimators. Finally, Section VI provides some concluding remarks.

II. M-to-M Channel Model

This section briefly reviews our model [14] for noisy Ricean narrow-band SISO M-to-M multipath fading channels. Fig. 1 shows our "two-ring" geometrical model [14] that characterizes an outdoor environment. It is assumed that both the $\mathrm{T_x}$ and $\mathrm{R_x}$ are in motion and equipped with low-elevation antennas. The radio propagation is modelled as 2-D non-isotropic scattering with either line-of-sight (LoS) or non-line-of-sight (NLoS) conditions between the $\mathrm{T_x}$ and $\mathrm{R_x}$. The two-ring model defines two rings of fixed scatterers, one around the $\mathrm{T_x}$ and another around the $\mathrm{R_x}$, as shown in Fig. 1. Around the transmitter, M omnidirectional scatterers lie on a ring of radius R_t, and the mth transmit scatterer is denoted by $S_T^{(m)}$. Similarly, N omnidirectional scatterers lie on a ring of radius R_r, around the receiver, and the nth receive scatterer is denoted by $S_R^{(n)}$.

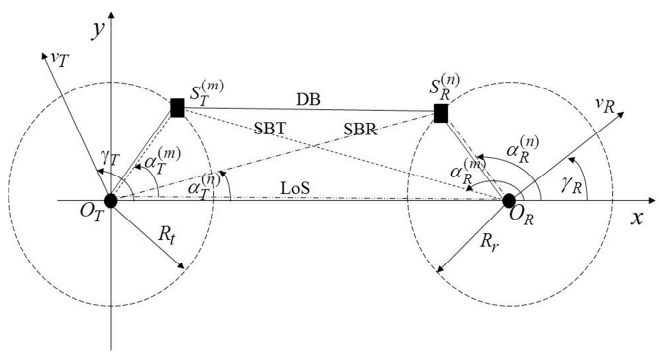

Fig. 1. Geometrical model for the SISO M-to-M channel.

The received complex faded envelope can be written as

$$r(t) = h^d(t) + h^{LoS}(t) + n(t), \tag{1}$$

where the complex Gaussian process $n(t)$ represents the received noise, $h^{LoS}(t)$ represents the deterministic line-of-sight (LoS) component of the received complex faded envelope, and the complex process $h^d(t)$ represents the random diffuse (multipath) component of the received complex faded envelope. The LoS component of the received complex faded envelope is

$$h^{LoS}(t) = \sqrt{\frac{K}{K+1}} e^{jt\omega_{T\max}\cos(\gamma_T) + jt\omega_{R\max}\cos(\pi-\gamma_R)}. \tag{2}$$

The multipath component of the received complex faded envelope can be written as a superposition of the single-bounced transmit, single-bounced receive, and double-bounced rays [14], i.e.,

$$h^d(t) = h^{SBT}(t) + h^{SBR}(t) + h^{DB}(t), \tag{3}$$

where the single-bounced components are, respectively,

$$h^{SBT}(t) = \sqrt{\frac{\eta_T}{K+1}} \sum_{m=1}^{M} e^{j\phi_m} \times e^{jt\left[\omega_{T\max}\cos(\alpha_T^{(m)}-\gamma_T)+\omega_{R\max}\cos(\alpha_R^{(m)}-\gamma_R)\right]}, \tag{4}$$

$$h^{SBR}(t) = \sqrt{\frac{\eta_R}{K+1}} \sum_{n=1}^{N} e^{j\phi_n} \times e^{jt\left[\omega_{T\max}\cos(\alpha_T^{(n)}-\gamma_T)+\omega_{R\max}\cos(\alpha_R^{(n)}-\gamma_R)\right]}, \tag{5}$$

and the double-bounced component is

$$h^{DB}(t) = \sqrt{\frac{\eta_{TR}}{K+1}} \sum_{m,n=1}^{M,N} e^{j\phi_{mn}} \times e^{jt\left[\omega_{T\max}\cos(\alpha_T^{(m)}-\gamma_T)+\omega_{R\max}\cos(\alpha_R^{(n)}-\gamma_R)\right]}. \tag{6}$$

In (2)–(6), K denotes the Ricean factor, and η_T, η_R, and η_{TR} specify how much the single- and double-bounced rays contribute in the total averaged power $\mathrm{E}[|h^d(t)|^2]$, i.e., these parameters satisfy $\eta_T+\eta_R+\eta_{TR}=1$. The $\mathrm{T_x}$ and the $\mathrm{R_x}$ are moving with speeds v_T and v_R, and in directions described by angles γ_T and γ_R, respectively, as shown in Fig. 1. Angular frequencies $\omega_{T\max} = 2\pi v_T/\lambda$ and $\omega_{R\max} = 2\pi v_R/\lambda$ are the maximum Doppler angular frequencies associated with the $\mathrm{T_x}$ and the $\mathrm{R_x}$, respectively, and λ is the carrier wavelength. Symbols $\alpha_T^{(m)}$ and $\alpha_T^{(n)}$ denote the angles of departure (AoD), whereas $\alpha_R^{(m)}$ and $\alpha_R^{(n)}$ denote the angles of arrival (AoA). Note that double-bounced rays have the AoD, $\alpha_T^{(m)}$, independent from the AoA, $\alpha_R^{(n)}$, whereas single-bounced rays have the AoA, $\alpha_R^{(m)}$, dependent on the AoD, $\alpha_T^{(m)}$, and the AoD, $\alpha_T^{(n)}$, dependent on the AoA $\alpha_R^{(n)}$ [14]. The phases ϕ_m, ϕ_n, and ϕ_{mn} are random variables uniformly distributed on the interval $[-\pi,\pi)$, whereas the AoDs and AoAs are random variables with von Mises probability density functions [16], i.e., $p(\alpha_T) = \exp\left[k_T\cos(\alpha_T-\mu_T)\right]/(2\pi I_0(k_T))$ and $p(\alpha_R) = \exp\left[k_R\cos(\alpha_R-\mu_R)\right]/(2\pi I_0(k_R))$, respectively. Parameters $\mu_{T(R)} \in [-\pi,\pi)$ are the mean angles at which the scatterers are distributed in the horizontal plane, $k_{T(R)}$ control the spread of scatterers around the means, and $I_0(\cdot)$ is the zeroth-order modified Bessel function of the first kind. We use this pdf because it models both isotropic and non-isotropic environments and leads to closed-form solutions for many useful situations.

III. Estimation of $\mathrm{T_x}$ and $\mathrm{R_x}$ Velocities

This section derives closed-form expressions for the joint estimation of $\mathrm{T_x}$ and $\mathrm{R_x}$ velocities, and proposes a practical estimation algorithm that guaranties non-negative, non-complex values for the estimated velocities and improves the estimator performance.

To derive closed-form expressions for the estimation of $\mathrm{T_x}$ and $\mathrm{R_x}$ velocities, we assume a noise-free isotropic scattering environment with no LoS component. In Section V we will show that the effects of non-isotropic scattering, LoS propagation, and Gaussian noise do not significantly impact the performance of the proposed estimator. In the absence of noise and LoS component, i.e., $n(t)=0$ and $K=0$, the received complex faded envelope $r(t)$ is equal to the multipath component of the channel impulse response $h^d(t)$, i.e., $r(t)=h^d(t)$. Furthermore, since the $\mathrm{T_x}$ and $\mathrm{R_x}$ velocities v_T and v_R are proportional to the maximum Doppler angular frequencies $\omega_{T\max}$ and $\omega_{R\max}$, respectively, in the rest of the

paper we will focus on the estimation of $\omega_{T\max}$ and $\omega_{R\max}$ to simplify the notation.

To estimate the $\mathrm{T_x}$ and $\mathrm{R_x}$ angular frequencies $\omega_{T\max}$ and $\omega_{R\max}$, we combine the number of zero-crossings with the number of maxima in the in-phase component of $h^d(t)$ (i.e., $h_i^d(t) = \Re\{h^d(t)\}$) and in the quadrature component of $h^d(t)$ (i.e., $h_q^d(t) = \Im\{h^d(t)\}$). Here, $\Re\{\cdot\}$ denotes the real part operation and $\Im\{\cdot\}$ denotes the imaginary part operation. The in-phase and quadrature components of $h^d(t)$ are observed over a time interval of length T. We choose this crossing-based estimation approach because it does not depend on the type of propagation environment, i.e., it does not depend on the parameters η_T, η_R, and η_{TR}.

Let us define $L_{h_i^d}(0,T)$ as the count of how many times the in-phase component $h_i^d(t)$ crosses the zero-level threshold with a positive slope, counted over the time interval $(0,T]$. Similarly, $L_{h_q^d}(0,T)$ is the count of positive-slope zero-level crossings for the quadrature component $h_q^d(t)$ counted over the time interval $(0,T]$. Also, we define $M_{h_i^d}(T)$ as the number of maxima in $h_i^d(t)$ during the time interval $(0,T]$. Similarly, $M_{h_q^d}(T)$ is the number of maxima in $h_q^d(t)$ during the time interval $(0,T]$.

Here we note that the $h_i^d(t)$ and $h_q^d(t)$ are stationary Gaussian processes with zero means. This can be shown by noting that the cosine and sine functions in the sums of $h_i^{SBT}(t) = \Re\{h^{SBT}(t)\}$ and $h_q^{SBT}(t) = \Im\{h^{SBT}(t)\}$ are statistically independent and identically distributed random variables with zero mean and a finite variance. According to the central limit theorem [6], for $M \to \infty$, $h_i^{SBT}(t)$ and $h_q^{SBT}(t)$ are stationary Gaussian processes with zero means. Similarly, for $N \to \infty$, $h_i^{SBR}(t) = \Re\{h^{SBR}(t)\}$ and $h_q^{SBR}(t) = \Im\{h^{SBR}(t)\}$ are stationary Gaussian processes with zero means. When the channel does not experience keyhole behavior (the assumption included in our model [14]) and $M, N \to \infty$, $h_i^{DB}(t) = \Re\{h^{DB}(t)\}$ and $h_q^{DB}(t) = \Im\{h^{DB}(t)\}$ are also stationary Gaussian processes with zero means. Using similar reasoning, we can conclude that the linear combinations of $h_{i(q)}^{SBT}(t)$, $h_{i(q)}^{SBR}(t)$, $h_{i(q)}^{DB}(t)$, i.e., $h_i^d(t)$ and $h_q^d(t)$, are also stationary Gaussian processes with zero means.

Then, for stationary zero-mean Gaussian processes $h_i^d(t)$ and $h_q^d(t)$, the number of zero crossings can be written as [7]

$$\mathrm{E}[L_{h_i^d}(0,T)] = \mathrm{E}[L_{h_q^d}(0,T)] = \frac{T}{2\pi}\sqrt{\frac{b_2}{b_0}}, \tag{7}$$

and the number of maxima can be written as [7]

$$\mathrm{E}[M_{h_i^d}(T)] = \mathrm{E}[M_{h_q^d}(T)] = \frac{T}{2\pi}\sqrt{\frac{b_4}{b_2}}. \tag{8}$$

The parameters b_0, b_2, and b_4 are defined as [17]

$$b_0 \triangleq \mathrm{E}[h_i^d(t)^2] = \mathrm{E}[h_q^d(t)^2], \tag{9}$$

$$b_2 \triangleq \mathrm{E}[\dot{h}_i^d(t)^2] = \mathrm{E}[\dot{h}_q^d(t)^2], \tag{10}$$

$$b_4 \triangleq \mathrm{E}[\ddot{h}_i^d(t)^2] = \mathrm{E}[\ddot{h}_q^d(t)^2], \tag{11}$$

where $\mathrm{E}[\cdot]$ denotes the statistical expectation operator, $\dot{h}_i^d(t)$ and $\dot{h}_q^d(t)$ denote the first derivative of $h_i^d(t)$ and $h_q^d(t)$ with respect to time t, and $\ddot{h}_i^d(t)$ and $\ddot{h}_q^d(t)$ denote the second derivative of $h_i^d(t)$ and $h_q^d(t)$ with respect to time t.

Substituting (3) into (9), (10), and (11), respectively, finding the expectations with respect to all random variables (i.e., the angles of arrival, angles or departure, and phases), and after lengthy derivations, we obtain the following expressions for parameters b_0, b_2, and b_4

$$b_0 = \frac{1}{2(K+1)}, \tag{12}$$

$$b_2 \approx \frac{b_0}{2} \times \left[(1+\eta_R\cos(2\gamma_T))\omega_{T\max}^2 + (1+\eta_T\cos(2\gamma_R))\omega_{R\max}^2\right], \tag{13}$$

$$b_4 \approx b_0\Bigg[\left[\frac{3}{8}+\eta_R\left(\cos^4\gamma_T-\frac{3}{8}\right)\right]\omega_{T\max}^4 + \times\, b_0\left[\frac{3}{8}+\eta_T\left(\cos^4\gamma_R-\frac{3}{8}\right)\right]\omega_{R\max}^4 + 3b_0\omega_{R\max}^2\omega_{T\max}^2 \times \left[0.5+\eta_T(\cos^2\gamma_R-0.5)+\eta_R(\cos^2\gamma_T-0.5)\right]\Bigg]. \tag{14}$$

Here we note that, for each connection between two mobile terminals, the direction angles γ_T and γ_R are deterministic quantities. In all previous velocity estimation algorithms [6]-[10], it is assumed that $\gamma_T = \gamma_R = 0$, so that the velocity estimation does not depend on direction angles. This is not a good assumption when estimating both velocities. Instead, we propose to remove the dependence between the velocities and the direction angles by assuming that all directions are equally probable, i.e., angles γ_T and γ_R can be treated as random variables with a uniform distribution over $(0, 2\pi]$. Averaging over all possible values of γ_T and γ_R, we obtain the following expressions for b_2 and b_4, respectively,

$$b_2 = \frac{b_0}{2}\left[\omega_{T\max}^2 + \omega_{R\max}^2\right], \tag{15}$$

$$b_4 = b_0\left[\frac{3}{8}\omega_{T\max}^4 + \frac{3}{8}\omega_{R\max}^4 + \frac{3}{2}\omega_{R\max}^2\omega_{T\max}^2\right]. \tag{16}$$

Substituting (12), (15), and (16) into (7) and (8), the number of zero crossings and the number of maxima in $h_i^d(t)$ or $h_q^d(t)$ become, respectively,

$$\mathrm{E}[L_{h_i^d}(0,T)] = \mathrm{E}[L_{h_q^d}(0,T)] = \frac{T}{2\sqrt{2}\pi}\sqrt{\omega_{T\max}^2+\omega_{R\max}^2} \tag{17}$$

$$\mathrm{E}[M_{h_i^d}(T)] = \mathrm{E}[M_{h_q^d}(T)] = \frac{T}{2\pi} \times \sqrt{\frac{\frac{3}{8}\omega_{T\max}^4 + \frac{3}{8}\omega_{R\max}^4 + \frac{3}{2}\omega_{T\max}^2\omega_{R\max}^2}{\frac{1}{2}\omega_{T\max}^2 + \frac{1}{2}\omega_{R\max}^2}}. \tag{18}$$

Solving this set of equations with respect to $\omega_{T\max}$ and $\omega_{R\max}$, we obtain the following expressions for potential estimators:

$$\hat{\omega}_{T_i} = \frac{2\pi}{T} \times \sqrt{L_{h_i^d}(0,T)^2 + \sqrt{3L_{h_i^d}(0,T)^4 - 4L_{h_i^d}(0,T)^2 M_{h_i^d}(T)^2/3}}, \tag{19}$$

$$\hat{\omega}_{R_i} = \frac{2\pi}{T} \times \sqrt{L_{h_i^d}(0,T)^2 - \sqrt{3L_{h_i^d}(0,T)^4 - 4L_{h_i^d}(0,T)^2 M_{h_i^d}(T)^2/3}}, \tag{20}$$

$$\hat{\omega}_{T_q} = \frac{2\pi}{T} \times \sqrt{L_{h_q^d}(0,T)^2 + \sqrt{3L_{h_q^d}(0,T)^4 - 4L_{h_q^d}(0,T)^2 M_{h_q^d}(T)^2/3}}, \tag{21}$$

$$\hat{\omega}_{R_q} = \frac{2\pi}{T} \times \sqrt{L_{h_q^d}(0,T)^2 - \sqrt{3L_{h_q^d}(0,T)^4 - 4L_{h_q^d}(0,T)^2 M_{h_q^d}(T)^2/3}}. \tag{22}$$

Using the approximation $\mathrm{E}[x] \approx \sqrt{\mathrm{E}[x^2]}$ in [18], Appendix A shows that these estimators are approximately unbiased, i.e., $\mathrm{E}[\hat{\omega}_{T_{i(q)}}] \approx \omega_{T\max}$ and $\mathrm{E}[\hat{\omega}_{R_{i(q)}}] \approx \omega_{R\max}$.

While testing the estimators in (19)-(22), we observed that it is not clear if the estimator in (19) outperforms the estimator in (21) or vice versa. Furthermore, we noted that the estimated velocities have to have non-negative, non-complex values. To ensure that the estimated velocities have non-negative, non-complex values and to capture the best performance between the estimators in (19) and (21), we empirically find that combining the estimators in (19) and (21) as described in the following algorithm leads to the best results. If $\Re\left\{\sqrt{3L_{h_i^d}(0,T)^4/T^4 - 4L_{h_i^d}(0,T)^2 M_{h_i^d}(T)^2/(3T^4)}\right\} < 2$ or $\Re\left\{\sqrt{3L_{h_q^d}(0,T)^4/T^4 - 4L_{h_q^d}(0,T)^2 M_{h_q^d}(T)^2/(3T^4)}\right\} < 2$, the angular velocity $\hat{\omega}_T$ is estimated as

$$\hat{\omega}_T = \Re\left\{\sqrt{\min\left(\hat{\omega}_{Ti}^2, \hat{\omega}_{Tq}^2\right)}\right\}, \tag{23}$$

where $\hat{\omega}_{Ti}$ and $\hat{\omega}_{Tq}$ are defined as in (19) and (21), respectively, and $\min(\cdot)$ denotes the minimum function. On the other hand, if $\Re\left\{\sqrt{3L_{h_i^d}(0,T)^4/T^4 - 4L_{h_i^d}(0,T)^2 M_{h_i^d}(T)^2/(3T^4)}\right\} \geq 2$ or $\Re\left\{\sqrt{3L_{h_q^d}(0,T)^4/T^4 - 4L_{h_q^d}(0,T)^2 M_{h_q^d}(T)^2/(3T^4)}\right\} \geq 2$, the angular Doppler frequency $\hat{\omega}_T$ is estimated as

$$\hat{\omega}_T = \Re\left\{\sqrt{\max\left(\hat{\omega}_{Ti}^2, \hat{\omega}_{Tq}^2\right)}\right\}, \tag{24}$$

where $\max(\cdot)$ denotes the maximum function. Using the obtained results , the angular Doppler frequency $\hat{\omega}_R$ is estimated as

$$\hat{\omega}_R = \Re\left\{\sqrt{\frac{4}{T^2}[\max(\mathrm{E}[L_{h_i^d}(0,T)], \mathrm{E}[L_{h_q^d}(0,T)])]^2 - \mathrm{E}[\hat{\omega}_T]^2}\right\}. \tag{25}$$

IV. Estimation of Relative Direction of Movement of $\mathrm{T_x}$ and $\mathrm{R_x}$

This section derives the closed-form expression for estimating the relative direction of movement of $\mathrm{T_x}$ and $\mathrm{R_x}$. Here, we assume a noise-free, non-isotropic scattering environment with a LoS component. In Section V we will evaluate the effect of Gaussian noise on the performance of the proposed estimator.

To estimate the relative direction of movement of $\mathrm{T_x}$ and $\mathrm{R_x}$, we use the cross-correlation between the in-phase component of $h(t)$ (i.e., $h_i(t) = \Re\{h(t)\}$) and the quadrature component of $h(t)$ (i.e., $h_q(t) = \Im\{h(t)\}$). The cross-correlation between the in-phase and and quadrature component of $h(t)$ can be written as [14]

$$R^{IQ}(\tau) = R^{IQ}_{LoS}(\tau) + R^{IQ}_{SBT}(\tau) + R^{IQ}_{SBR}(\tau) + R^{IQ}_{DB}(\tau), \tag{26}$$

where

$$R^{IQ}_{LoS}(\tau) = \frac{0.5K}{K+1}\sin(\omega_T\tau\cos\gamma_T - \omega_R\tau\cos\gamma_R), \tag{27}$$

$$R^{IQ}_{SBT}(\tau) = \frac{0.5\eta_T}{K+1}\sin(\tau\omega_{R\max}\cos\gamma_R) \times \Re\left\{\frac{I_0\left(\sqrt{k_T^2 - \tau^2\omega_{T\max}^2 - j2k_T\tau\omega_{T\max}\cos(\mu_T-\gamma_T)}\right)}{I_0(k_T)}\right\} + \frac{0.5\eta_T}{K+1}\cos(\tau\omega_{R\max}\cos\gamma_R) \times \Im\left\{\frac{I_0\left(\sqrt{k_T^2 - \tau^2\omega_{T\max}^2 - j2k_T\tau\omega_{T\max}\cos(\mu_T-\gamma_T)}\right)}{I_0(k_T)}\right\}, \tag{28}$$

$$R^{IQ}_{SBR}(\tau) = \frac{-0.5\eta_R}{K+1}\sin(\tau\omega_{T\max}\cos\gamma_T) \times \Re\left\{\frac{I_0\left(\sqrt{k_R^2 - \tau^2\omega_{R\max}^2 - j2k_R\tau\omega_{R\max}\cos(\mu_R-\gamma_R)}\right)}{I_0(k_R)}\right\} + \frac{0.5\eta_R}{K+1}\cos(-\tau\omega_{T\max}\cos\gamma_T) \times \Im\left\{\frac{I_0\left(\sqrt{k_R^2 - \tau^2\omega_{R\max}^2 - j2k_R\tau\omega_{R\max}\cos(\mu_R-\gamma_R)}\right)}{I_0(k_R)}\right\}, \tag{29}$$

$$R^{IQ}_{DB}(\tau) = \frac{0.5\eta_{TR}}{K+1} \times \Im\left\{\frac{I_0\left(\sqrt{k_T^2 - \tau^2\omega_{T\max}^2 - j2k_T\tau\omega_{T\max}\cos(\mu_T-\gamma_T)}\right)}{I_0(k_T)}\right\} \times \Re\left\{\frac{I_0\left(\sqrt{k_R^2 - \tau^2\omega_{R\max}^2 - j2k_R\tau\omega_{R\max}\cos(\mu_R-\gamma_R)}\right)}{I_0(k_R)}\right\} + \frac{0.5\eta_{TR}}{K+1} \times \Re\left\{\frac{I_0\left(\sqrt{k_T^2 - \tau^2\omega_{T\max}^2 - j2k_T\tau\omega_{T\max}\cos(\mu_T-\gamma_T)}\right)}{I_0(k_T)}\right\} \times \Im\left\{\frac{I_0\left(\sqrt{k_R^2 - \tau^2\omega_{R\max}^2 - j2k_R\tau\omega_{R\max}\cos(\mu_R-\gamma_R)}\right)}{I_0(k_R)}\right\}. \tag{30}$$

For a small time-lag $\tau \to 0$, the cross-correlation function in (26) can be approximated as

$$R^{IQ}(\tau) \approx \frac{0.5}{K+1}\Big[K\omega_T\tau\cos\gamma_T - K\omega_R\tau\cos\gamma_R + \eta_T\tau$$

$$\times\ \omega_{R\max}\cos\gamma_R - \eta_R\tau\omega_{T\max}\cos\gamma_T + (\eta_R+\eta_{TR})\Im\{B\}\Big], \tag{31}$$

where $B = I_0(\sqrt{k_R^2 - \tau^2\omega_{R\max}^2 - j2k_R\tau\omega_{R\max}\cos(\mu_R-\gamma_R)})$ $/I_0(k_R)$. The derivation of this approximation is presented in Appendix B.

Without loss of generality, we assume that the coordinate system is aligned with the receiver, i.e., $\gamma_R = 0$ and that the angle γ_T represents the relative direction of movement of $\mathrm{T_x}$ and $\mathrm{R_x}$. Then, (31) can be simplified to

$$R^{IQ}(\tau) = \frac{0.5}{K+1}\Big[K\omega_T\tau\cos\gamma_T - K\omega_R\tau + \eta_T\tau\omega_{R\max} - \eta_R\tau\omega_{T\max}\cos\gamma_T + (\eta_R+\eta_{TR})\Im\{B\}\Big]. \tag{32}$$

Finally, solving (32) with respect to γ_T, the relative direction of movement of $\mathrm{T_x}$ and $\mathrm{R_x}$ is estimated as

$$\hat{\gamma}_T = \arccos\left(\frac{-2(K+1)R^{IQ}(\tau) + \eta_T\hat{\omega}_R\tau}{\eta_R\hat{\omega}_T\tau - K\hat{\omega}_T\tau} + \frac{-K\hat{\omega}_R\tau + (\eta_T+\eta_{TR})\Im\{\hat{B}\}}{\eta_R\hat{\omega}_T\tau - K\hat{\omega}_T\tau}\right), \tag{33}$$

where $0 \le \hat{\gamma}_T \le 180°$ and the angular Doppler frequencies $\hat{\omega}_T$ and $\hat{\omega}_R$ are estimated using (23)-(24) and (25), respectively.

V. Performance Analysis

This section presents the performance analysis of the proposed estimation algorithms. First, we evaluate the proposed estimation algorithms in a noise-free isotropic scattering environment with no LoS component, and then we study the effect of non-isotropic scattering, LoS propagation, and Gaussian noise on the performance of the proposed estimators.

The estimation error for the velocities estimator is evaluated using the root mean square error (RMSE) given by

$$\mathrm{E}[(\hat{f}_{T(R)} - f_{T\max(R\max)})^2]^{1/2} = \left(\mathrm{Var}[\hat{f}_{T(R)}] + (\mathrm{E}[\hat{f}_{T(R)}] - f_{T\max(R\max)})^2\right)^{1/2}, \tag{34}$$

where $\mathrm{Var}[\cdot]$ denotes the variance operation, $(\mathrm{E}[\hat{f}_{T(R)}] - f_{T\max(R\max)})^2$ represents the bias, and $\hat{f}_{T(R)} = \hat{\omega}_{T(R)}/(2\pi)$ and $f_{T\max(R\max)} = \omega_{T\max(R\max)}/(2\pi)$ denote the estimated and actual Doppler frequencies at the $\mathrm{T_x}$ and the $\mathrm{R_x}$, respectively. The estimation error for the direction estimator is evaluated using the RMSE given by

$$\mathrm{E}[(\hat{\gamma}_T - \gamma_T)^2]^{1/2} = \left(\mathrm{Var}[\hat{\gamma}_T] + (\mathrm{E}[\hat{\gamma}_T] - \gamma_T)^2\right)^{1/2}, \tag{35}$$

where $(\mathrm{E}[\hat{\gamma}_T] - \gamma_T)^2$ represents the bias. Using our "deterministic" channel simulator [14] with $M = 30$ scatterers around the $\mathrm{T_x}$ and $N = 30$ scatterers around the $\mathrm{R_x}$, 10,000 independent realizations of complex Gaussian processes are generated. Each realization is of $T = 1$ s duration, i.e., it has $S = 10,000$ samples.

Fig. 2 shows the RMSE of the estimated $\mathrm{T_x}$ Doppler frequency $\hat{f}_T$ versus the actual $\mathrm{T_x}$ Doppler frequency $f_{T\max}$, for several different $\mathrm{R_x}$ Doppler frequencies $f_{R\max} = \{0, 10, 30, 60, 90\}$ Hz, in a noise-free, isotropic scattering environment with no LoS component. An estimate of the $\mathrm{T_x}$ Doppler frequency is obtained for each individual channel realization, and then all 10,000 realizations are used to calculate the RMSE. Fig. 2 shows that the proposed single-velocity estimation algorithm is highly accurate. To illustrate how our single-velocity estimator in (23)-(24) compares with the estimators in [7], Fig. 2 also plots the RMSE of the the number of maxima in the in-phase component of the channel impulse response estimator [7]. In [7], it has been shown that this

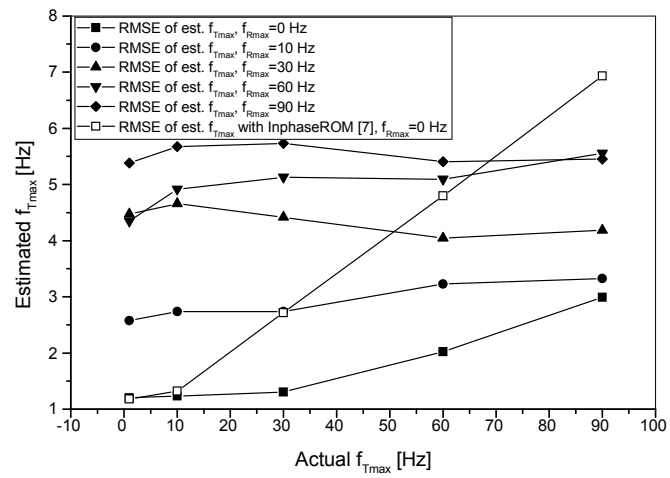

Fig. 2. The RMSE of the estimated Doppler frequency $\hat{f}_T$ versus the actual Doppler frequency $f_{T\max}$, in a noise-free isotropic scattering environment with no LoS component.

estimator outperforms level-crossing rate, the zero-crossing rate, the integration based, and the covariance based estimators, i.e., we compare our proposed estimator with the best-performing estimator from prior work. The results show that, if used to estimate only one velocity (i.e., $f_{R\max} = 0$), our velocities estimator outperforms the estimators compared in [7]. Our velocity estimator outperforms the existing estimators because it combines the zero-crossing rates with the number of maxima, and also because it uses both the in-phase and the quadrature components of the channel impulse response.

Fig. 3 shows the RMSE of the estimated $\mathrm{R_x}$ Doppler frequency $\hat{f}_R$ versus the actual $\mathrm{R_x}$ Doppler frequency $f_{R\max}$, for several different $\mathrm{T_x}$ Doppler frequencies $f_{T\max} = \{1, 10, 30, 60, 90\}$ Hz, in a noise-free isotropic scattering environment with no LoS component. An estimate of the $\mathrm{R_x}$ Doppler frequency is obtained using 20 channel realizations, and the RMSE is obtained by averaging over 500 different estimations of $\hat{f}_R$. The results in Fig 3 show that the proposed velocities estimation algorithm is highly accurate. However, we can observe that the RMSE of the estimated Doppler frequency $\hat{f}_R$ is higher than the RMSE of the estimated Doppler frequency $\hat{f}_T$. This is due to increase in the bias. While the estimation of the Doppler frequency $\hat{f}_T$ is approximately unbiased, the estimation of the Doppler frequency $\hat{f}_R$ depends on the result obtained for $\hat{f}_T$ (see (25)). However, Figure 3 shows that this bias is relatively small.

Fig. 4 shows the RMSE of the estimated direction of

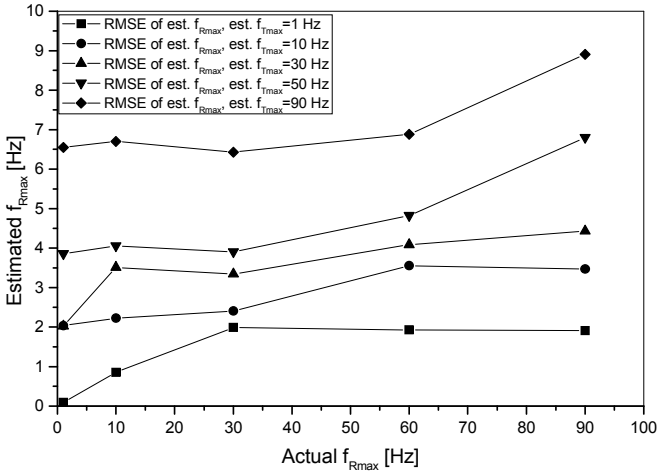

Fig. 3. The RMSE of the estimated Doppler frequency $\hat{f}_R$ versus the actual Doppler frequency $f_{R\max}$, in a noise-free isotropic scattering environment with no LoS component.

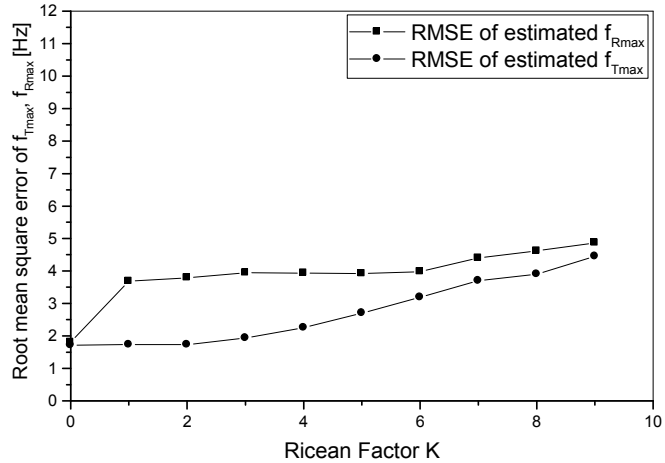

Fig. 5. The RMSE of estimated Doppler frequencies $\hat{f}_T$ and $\hat{f}_R$ versus Ricean factor K, in a noise-free isotropic scattering environment with a LoS component, for $f_{T\max} = 10$ Hz and $f_{R\max} = 20$ Hz.

movement of $\mathrm{T_x}$ and $\mathrm{R_x}$, i.e., $\hat{\gamma}_T$ versus the actual direction γ_T in a noise-free isotropic scattering environment with no LoS component. Here, we run simulations with several actual and estimated $\mathrm{T_x}$ and $\mathrm{R_x}$ Doppler frequencies $f_{T\max} = f_{R\max} = \{1, 10, 50, 90\}$ Hz. When using the actual Doppler frequencies, the RMSE is zero. However, this is not a realistic assumption. Hence, in Fig. 4 we plot the results obtained with the estimated velocities. The results show that the proposed estimation algorithm is very accurate: the largest RMSE does not exceed $5°$.

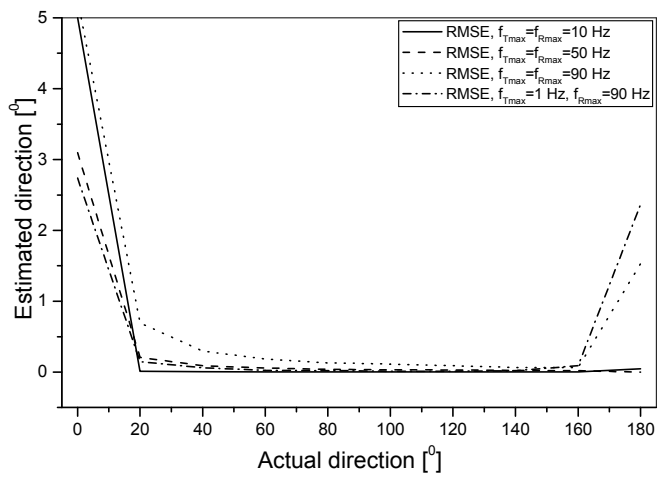

Fig. 4. The RMSE of the estimated direction $\hat{\gamma}_T$ versus the actual direction γ_T, in a noise-free isotropic scattering environment with no LoS component.

Fig. 5 illustrates the effect of the LoS component (i.e., Ricean parameter K) on the performance of the proposed *velocities estimator*. Here, we assume a noise-free isotropic scattering environment with $f_{T\max} = 10$ Hz and $f_{R\max} = 20$ Hz. The results show that both estimated Doppler frequencies ($\hat{f}_T$ and $\hat{f}_R$) are fairly insensitive to variations in the Ricean factor K. The RMSE of the $\mathrm{R_x}$ Doppler frequency is higher than the RMSE of the $\mathrm{T_x}$ Doppler frequency due to higher bias.

Fig. 6 shows the effect of the LoS component on the performance of the proposed *direction estimator*. Here, we assume a noise-free isotropic scattering environment with $f_{T\max} = f_{R\max} = 100$ Hz. Note that we use estimated angular velocities to calculate the RMSE of direction estimation. The RMSE is calculated for several directions $\gamma_T = \{0°, 40°, 80°, 90°, 100°, 140°, 180°\}$. The results show that the estimated direction is relatively insensitive to the variation of the Ricean factor K. The RMSE varies between $1°$ and $3°$. It is the highest for $\gamma_T = 90°$ due to obstruction in line-of-sight.

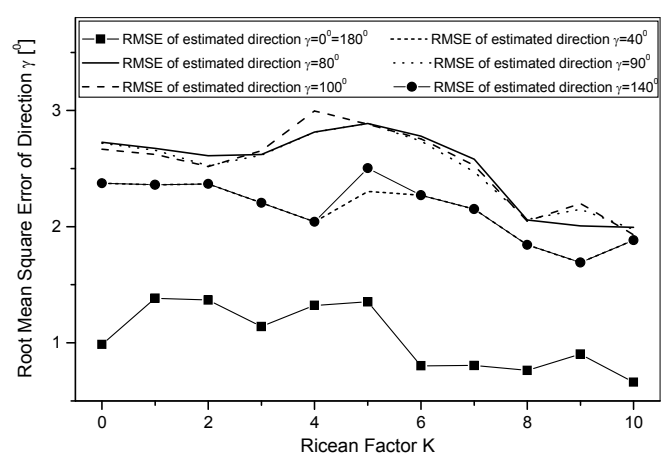

Fig. 6. The RMSE of the estimated direction $\hat{\gamma}_T$ versus Ricean factor K, in a noise-free isotropic scattering environment with a LoS component, for $f_{T\max} = 100$ Hz and $f_{R\max} = 100$ Hz.

Figs. 7 and 8 show the effect of a non-isotropic scattering on the performance of proposed *velocities estimator*. In these plots, a noise-free non-isotropic scattering environment with no LoS component is assumed, with $f_{T\max} = 10$ Hz and $f_{R\max} = 20$ Hz. Fig. 7 plots the RMSE of the estimated Doppler frequencies $\hat{f}_T$ and $\hat{f}_R$ versus the spread of the $\mathrm{T_x}$ scatterers around the mean value, i.e., k_T, for several different values of k_R, i.e., $k_R \in \{0, 3, 5, 10\}$. The mean angles at which the scatterers are distributed are $\mu_T = \mu_R = 0°$.

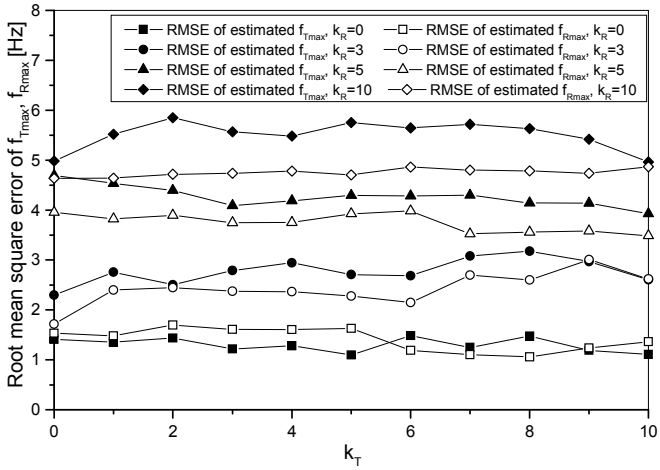

Fig. 7. The RMSE of estimated Doppler frequencies $\hat{f}_T$ and $\hat{f}_R$ versus k_T, in a noise-free non-isotropic scattering environment with no LoS component, for $f_{T\max} = 10$ Hz, $f_{R\max} = 20$ Hz, $\mu_T = \mu_R = 0°$, and $k_R \in \{0, 3, 5, 10\}$.

Fig. 8 plots the RMSE of the estimated Doppler frequencies $\hat{f}_T$ and $\hat{f}_R$ versus the mean angle at which the $\mathrm{T_x}$ scatterers are distributed, i.e., μ_T for several different values of $\mu_R \in \{0°, 30°, 45°, 60°, 90°\}$. The parameters k_T and k_R are set to 2. The results in Figs. 7 and 8 show that the proposed estimator has robust performance in a non-isotropic scattering environment.

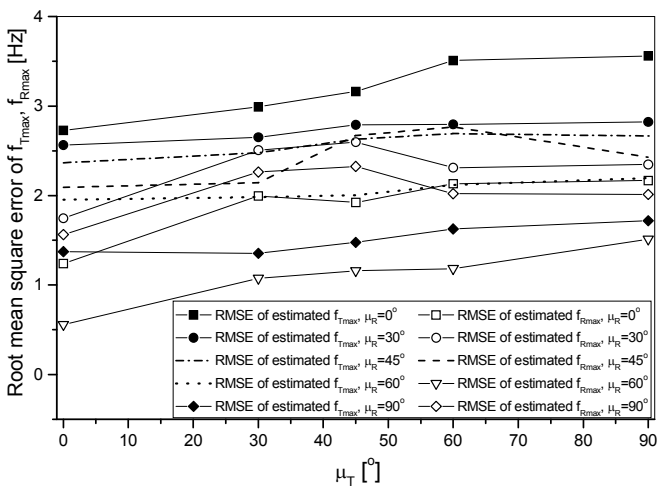

Fig. 8. The RMSE of estimated Doppler frequencies $\hat{f}_T$ and $\hat{f}_R$ versus μ_T, in a noise-free non-isotropic scattering environment with no LoS component, for $k_T = k_R = 2$, $f_{T\max} = 10$ Hz, $f_{R\max} = 20$ Hz, and $\mu_R \in \{0°, 30°, 45°, 60°, 90°\}$.

Figs. 9 and 10 show the effect of a non-isotropic scattering on the performance of the proposed *direction* estimator. In these plots, a noise-free non-isotropic scattering environment with no LoS component is assumed, and estimated results (from the velocities estimator) for Doppler frequencies $f_{T\max} = f_{R\max} = 100$ Hz are used. The RMSE is calculated for several directions $\gamma_T = \{0°, 40°, 80°, 90°, 100°, 140°, 180°\}$. Fig. 9 shows the RMSE of the estimated direction $\hat{\gamma}_T$ versus the spread of the $\mathrm{T_x}$ scatterers around the mean value, i.e., k_T. We have tested the estimator for several different spreads of the $\mathrm{R_x}$ scatterers, i.e., $k_R \in \{0, 3, 5, 10\}$, and the results are very similar in all cases. For brevity, we plot only

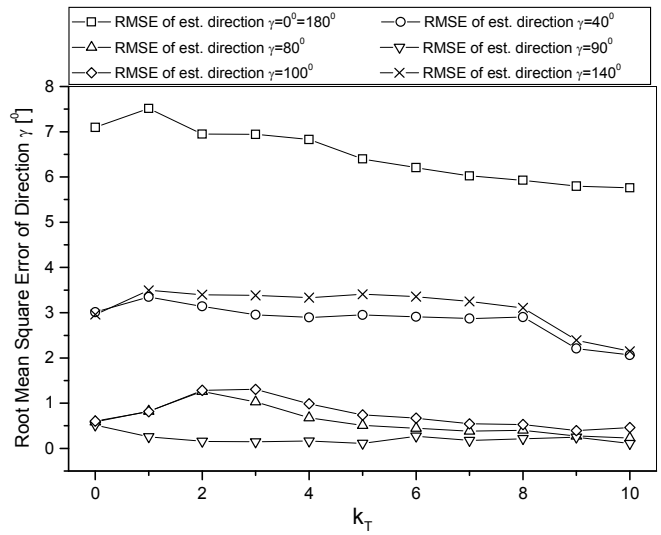

Fig. 9. The RMSE of the estimated direction $\hat{\gamma}_T$ versus k_T, in a noise-free non-isotropic scattering environment with no LoS component, for $f_{T\max} = f_{R\max} = 100$ Hz, and $k_R = 10$.

the results for $k_R = 10$. Fig. 10 plots the RMSE of the estimated direction $\hat{\gamma}_T$ versus the mean angle at which the $\mathrm{T_x}$ scatterers are distributed, i.e., μ_T. We have tested the estimator for several different values of $\mu_R \in \{0°, 45°, 90°, 135°, 180°\}$. Since the similar results are observed in all cases, here we plot only the results for $\mu_R = 90°$. The results in Figs. 9 and 10 show that the proposed estimator has robust performance in a non-isotropic scattering environment. Furthermore, we can observe that the RMSE in Fig. 10 varies between $1.5°$ and $2°$, while the RMSE in Fig. 9 has a larger spread (between $1°$ and $8°$). This result indicates that the estimation accuracy does depend on the relative position between the vehicles (i.e., the $\mathrm{T_x}$ and $\mathrm{R_x}$) and local scatterers, but the error does not exceed $10°$.

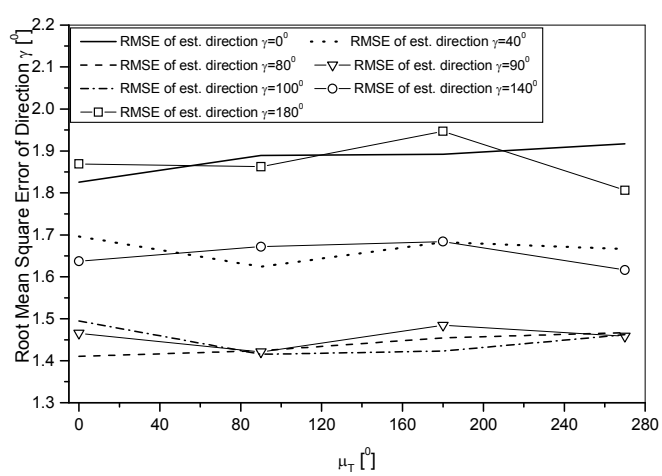

Fig. 10. The RMSE of the estimated direction $\hat{\gamma}_T$ versus μ_T, in a noise-free non-isotropic scattering environment with no LoS component, for $k_T = k_R = 10$, $f_{T\max} = f_{R\max} = 100$ Hz, and $\mu_R = 90°$.

In contrast to the velocities estimator, the direction estimator

depends on how much the single- and double-bounced rays contribute to the total averaged power, i.e., it depends on the parameters η_T, η_R, and η_{TR}. Fig. 11 shows the effect of the single- and double-bounced rays on the performance of the proposed direction estimator. Here, a noise-free non-isotropic scattering environment with no LoS component is assumed, and estimated Doppler frequencies $f_{T\max} = f_{R\max} = 100$ Hz are used. The RMSE is calculated for several directions $\gamma_T = \{0°, 40°, 80°, 90°, 100°, 140°, 180°\}$, and we assume $\eta_T = \eta_R$. The results show that the RMSE vary between $0.1°$ and $0.5°$, which indicates that the direction estimator is not sensitive to changes in the energy distribution of the single- and double-bounced rays.

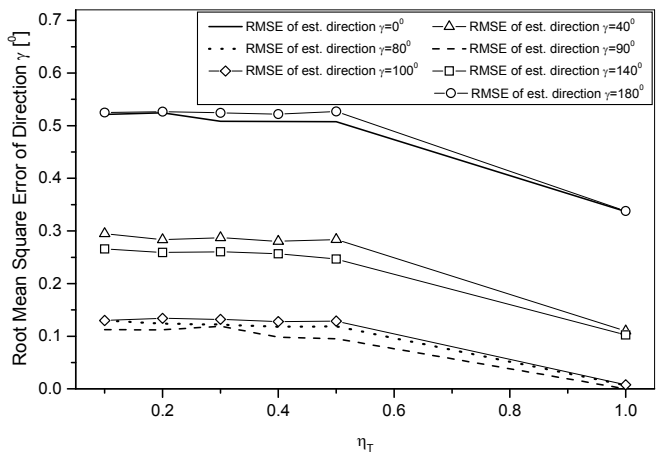

Fig. 11. The RMSE of the estimated direction $\hat{\gamma}_T$ versus η_T, in a noise-free isotropic scattering environment with no LoS component, for $f_{T\max} = f_{R\max} = 100$ Hz.

Finally, Figs. 12 and 13 illustrate the effect of white Gaussian noise on the proposed velocities estimator and the direction estimator, respectively. Here, an isotropic scattering environment with no LoS component is assumed. Fig. 12 plots the RMSE of estimated Doppler frequencies $\hat{f}_T$ and $\hat{f}_R$ versus actual Doppler frequencies, when signal-to-noise ratio is set to $\mathrm{SNR} = 10$ dB. The results show that the proposed velocities estimator performs relatively well in the presence of noise for all estimated velocities. Similarly, Fig. 13 plots the RMSE of the estimated direction $\hat{\gamma}_T$ versus the actual direction γ_T, when signal-to-noise ratio is $\mathrm{SNR} = \{5, 10, 15, 20\}$ dB and the estimated results for Doppler frequencies $f_{T\max} = f_{R\max} = 100$ Hz are selected. As expected, the performance of the direction estimator improves as the SNR increases. However, even for low SNR, e.g., $\mathrm{SNR} = 5$ dB, the RMSE does not exceed $15°$. Although a $15°$ error may not be acceptable for localization purposes, it can be tolerable in ad-hoc or energy-efficient routing algorithms, where only general orientation is needed (e.g., we typically need to know if vehicles are moving in the same, orthogonal, or opposite directions).

Overall, the results in Figs. 2- 13 show that the proposed velocities estimator and direction estimator provide very good estimation accuracy and perform well in the presence of a non-isotropic scattering, LoS propagation, and Gaussian noise.

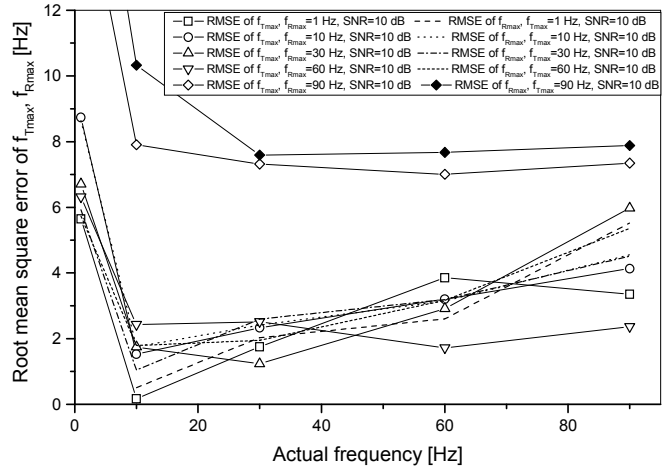

Fig. 12. The RMSE of estimated Doppler frequencies $\hat{f}_T$ and $\hat{f}_R$ versus the actual Doppler frequencies, in a noisy isotropic scattering environment with no LoS component and with $\mathrm{SNR} = 10$ dB.

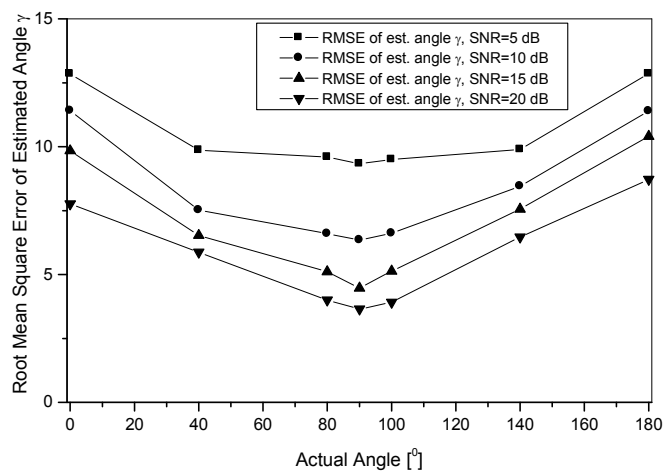

Fig. 13. The RMSE of the estimated direction $\hat{\gamma}_T$ versus the actual direction γ_T, in a noisy isotropic scattering environment with no LoS component and with $\mathrm{SNR} = \{5, 10, 15, 20\}$ dB.

VI. Conclusions

This paper proposed new estimators for mobile velocities and direction of movement in M-to-M wireless fading channels. First, we proposed the new crossing-based estimator that jointly estimates velocities of both the transmitter and the receiver in M-to-M communications. Then, we proposed the new correlation-based estimator that estimates the relative direction of movement of transmitter and receiver, using the estimated velocities in its computation. The proposed estimators are designed for narrow-band wireless M-to-M communications. They are evaluated through extensive computer simulations, and the results show that the proposed estimators provide very good estimation accuracy and perform well in the presence of a non-isotropic scattering, LoS propagation, and Gaussian noise.

Acknowledgment

The author would like to thank the anonymous reviewers whose feedback helped improve the quality of this paper.

Appendix A
Derivation of Biases for Estimators in Equations (19)-(22)

Using the approximation $\mathrm{E}[f(x)] \approx f(\mathrm{E}[x])$ in [18], where $f(x)$ denotes an arbitrary function, $\mathrm{E}[\hat{\omega}_{T_i}^2]$ and $\mathrm{E}[\hat{\omega}_{R_i}^2]$ can be approximated as

$$\mathrm{E}[\hat{\omega}_{T_i}^2] \approx \left(\frac{2\pi}{T}\right)^2 \Bigg[\mathrm{E}[L_{h_i^d}(0,T)]^2 \pm\sqrt{3\mathrm{E}[L_{h_i^d}(0,T)]^4 - 4\mathrm{E}[L_{h_i^d}(0,T)]^2\mathrm{E}[M_{h_i^d}(T)]^2/3}\Bigg], \quad (36)$$

$$\mathrm{E}[\hat{\omega}_{R_i}^2] \approx \left(\frac{2\pi}{T}\right)^2 \Bigg[\mathrm{E}[L_{h_i^d}(0,T)]^2 \mp\sqrt{3\mathrm{E}[L_{h_i^d}(0,T)]^4 - 4\mathrm{E}[L_{h_i^d}(0,T)]^2\mathrm{E}[M_{h_i^d}(T)]^2/3}\Bigg], \quad (37)$$

respectively. Substituting (17) and (18) into (36) and (37), $\mathrm{E}[\hat{\omega}_{T_i}^2]$ and $\mathrm{E}[\hat{\omega}_{R_i}^2]$ become, respectively,

$$\mathrm{E}[\hat{\omega}_{T_i}^2] \approx \omega_{T\max}^2, \quad (38)$$

$$\mathrm{E}[\hat{\omega}_{R_i}^2] \approx \omega_{R\max}^2. \quad (39)$$

Finally, using the approximation $\mathrm{E}[x] \approx \sqrt{\mathrm{E}[x^2]}$ in [18], we show that $\mathrm{E}[\hat{\omega}_{T_i}] \approx \omega_{T\max}$ and $\mathrm{E}[\hat{\omega}_{R_i}] \approx \omega_{R\max}$, respectively. Using similar reasoning, it can be shown that $\mathrm{E}[\hat{\omega}_{T_q}] \approx \omega_{T\max}$ and $\mathrm{E}[\hat{\omega}_{R_q}] \approx \omega_{R\max}$.

Appendix B
Derivation of Equation (31)

Using approximations $\sin x \approx x$, $\cos x \approx 1$, and $\sqrt{1+x} \approx 1 + x/2$, for small x, (26) can be approximated as follows

$$\begin{aligned} R^{IQ}(\tau) \approx{}& \frac{0.5K}{K+1}[\omega_T\tau\cos\gamma_T - \omega_R\tau\cos\gamma_R] + \frac{0.5\eta_T}{K+1} \\ &\times [\tau\omega_{R\max}\cos\gamma_R]\Re\left\{\frac{I_0(k_T(1-jY))}{I_0(k_T)}\right\} + \frac{0.5\eta_T}{K+1} \\ &\times \Im\left\{\frac{I_0\left(k_T(1-jY)\right)}{I_0(k_T)}\right\} - \frac{0.5\eta_R}{K+1}[\tau\omega_{T\max}\cos\gamma_T] \\ &\times \Re\left\{\frac{I_0(Z)}{I_0(k_R)}\right\} + \frac{0.5\eta_R}{K+1}\Im\left\{\frac{I_0\left(Z\right)}{I_0(k_R)}\right\} + \frac{0.5\eta_{TR}}{K+1} \\ &\times \Im\left\{\frac{I_0\left(k_T(1-jY)\right)}{I_0(k_T)}\right\}\Re\left\{\frac{I_0\left(Z\right)}{I_0(k_R)}\right\} + \frac{0.5\eta_{TR}}{K+1} \\ &\times \Re\left\{\frac{I_0\left(k_T(1-jY)\right)}{I_0(k_T)}\right\}\Im\left\{\frac{I_0\left(Z\right)}{I_0(k_R)}\right\}, \end{aligned} \quad (40)$$

where $Y = \tau\omega_{T\max}\cos(\mu_T - \gamma_T)/k_T$ and $Z = \sqrt{k_R^2 - \tau^2\omega_{R\max}^2 - j2k_R\tau\omega_{R\max}\cos(\mu_R - \gamma_R)}$. Then, using the equality [19, eq. 8.447], the approximation $[I_0(k_T(1-jY))]/I_0(k_T) \approx [1 + (k_T(1-jY))^2/4]/[1 + k_T^2/4]$ for $\tau \to 0$, and noting that $\Re\left\{I_0(Z)/I_0(k_R)\right\} = 1$, we obtain the expression in (31).

References

[1] J. Zhang, Q. Zhang, B. Li, X. Luo, and W. Zhu, "Energy-efficient routing in mobile and ad-hoc networks: mobility-assisted case," *IEEE Transactions on Vehicular Technology*, vol. 55, pp. 369–379, Jan. 2006.

[2] I. F. Akyildiz and W. Wang, "The predictive user mobility profile framework for wireless multimedia networks," *IEEE Transactions on Networking*, vol. 12, pp. 1021–1035, Dec. 2004.

[3] J. Holtzman and A. Sampath, "Adaptive averaging methodology for handoffs in cellular systems," *IEEE Transactions on Vehicular Technology*, vol. 44, pp. 59–66, Feb. 1995.

[4] M. J. Chu and W. E. Stark, "Effect of mobile velocity on communications in fading channels," *IEEE Transactions on Vehicular Technology*, vol. 49, pp. 202–210, Jan. 2000.

[5] L. Krasny, H. Arslan, D. Koilpillai, and S. Chennakeshu, "Doppler spread estimation in mobile radio systems," *IEEE Communication Letters*, vol. 5, pp. 197–199, May 2001.

[6] G. L. Stüber, *Principles of mobile communication 2e.* Kluwer, 2001.

[7] A. Abdi, H. Zhang, and C. Tepedelenlioglu, "A unified approach to the performance analysis of speed estimation techniques in mobile communication," *IEEE Transactions on Communications*, vol. 56, pp. 126–135, Jan. 2008.

[8] K. D. Anim-Appiah, "On generalized covariance-based velocity estimation," *IEEE Transactions on Vehicular Technology*, vol. 48, pp. 1546–1557, Sept. 1999.

[9] C. Xiao, K. D. Mann, and J. C. Olivier, "Mobile speed estimation for TDMA-based hierarchical cellular systems," *IEEE Transactions on Vehicular Technology*, vol. 50, pp. 981–991, July 2001.

[10] C. Tepedelenlioglu and G. B. Giannakis, "On velocity estimation and correlation properties of narrow-band mobile communication channels," *IEEE Transactions on Vehicular Technology*, vol. 50, pp. 1039–1052, July 2001.

[11] Y. R. Zheng and C. Xiao, "Mobile speed estimation for broadband wireless communications over rician fading channels," *IEEE Transactions on Wireless Communications*, vol. 8, pp. 1–5, Jan. 2009.

[12] K. Baddour and N. C. Beaulieu, "Nonparametric Doppler spread estimation for flat fading channels," *Proceedings of IEEE WCNC'03*, pp. 953–958, New Orleans, LA, USA, Mar. 2003.

[13] A. Dogandzic and B. Zhang, "Estimating Jakes' Doppler power spectrum parameters using the Whittle approximation," *IEEE Transactions on Signal Processing*, vol. 53, pp. 987–1005, March. 2005.

[14] A. G. Zajić and G. L. Stüber, "Space-time correlated mobile-to-mobile channels: modeling and simulation," *IEEE Transactions on Vehicular Technology*, vol. 57, pp. 715–726, Mar. 2008.

[15] A. G. Zajić, G. L. Stüber, T. G. Pratt, and S. Nguyen, "Wideband MIMO mobile-to-mobile channels: geometry-based statistical modeling with experimental verification," *IEEE Transactions on Vehicular Technology*, vol. 58, pp. 517–534, Feb. 2009.

[16] A. Abdi, J.A. Barger, and M. Kaveh, "A parametric model for the distribution of the angle of arrival and the associated correlation function and power spectrum at the mobile station," *IEEE Transactions on Vehicular Technology*, vol. 51, pp. 425–434, May 2002.

[17] W. C. Jakes, *Microwave Mobile Communications*, 2nd ed. Piscataway, NJ: Wiley-IEEE Press, 1994.

[18] G. Lindgren, "Spectral moment estimation by means of level crossings," *Biometrica*, vol. 61, pp. 401–418, Aug. 1974.

[19] I. S. Gradshteyn and I. M. Ryzhik, *Table of Integrals, Series, and Products* 5th *ed.*. A. Jeffrey, Ed. San Diego CA: Academic, 1994.

Alenka G. Zajić (S'99-M'08) received her B.Sc. and M.Sc. degrees from the School of Electrical Engineering, University of Belgrade, in 2001 and 2003, respectively. She received her Ph.D. degree in Electrical and Computer Engineering from the Georgia Institute of Technology in 2008. In 2010, she joined the School of Computer Science, Georgia Institute of Technology, where is visiting assistant professor. Her research interests are in wireless communications and applied electromagnetics.

Dr. Zajić received the Best Paper Award at ICT 2008, the Best Student Paper Award at WCNC 2007, and was also the recipient of the Dan Noble Fellowship in 2004, awarded by Motorola Inc. and IEEE Vehicular Technology Society for quality impact in the area of vehicular technology.